Journal of Membrane Science 596 (2020) 117726

Contents lists available at ScienceDirect

Journal of Membrane Science

journal homepage: http://www.elsevier.com/locate/memsci

# Intercalation of zwitterionic surfactants dramatically enhances the performance of low-pressure nanofiltration membrane

Yuanzhe Liang [a,b], Shihong Lin [a,b,c,*]

[a] Department of Civil and Environmental Engineering, Vanderbilt University, Nashville, TN, 37235, United States
[b] Interdisciplinary Material Science Program, Vanderbilt University, Nashville, TN, 37235, United States
[c] Department of Chemical and Biomolecular Engineering, Vanderbilt University, Nashville, TN, 37235, United States

ARTICLE INFO

*Keywords:*
Low-pressure nanofiltration
Layer-by-layer
Surfactant intercalation
Polyelectrolyte

ABSTRACT

High-performance nanofiltration membrane with excellent perm-selectivity and fouling resistance was fabricated by layer-by-layer deposition of polyelectrolytes, polyethylenimine (PEI) and polystyrene sulfonate (PSS), with the intercalation of self-assemblies of zwitterionic surfactants, 3-(*N, N*-Dimethylmyristylammonio) propane sulfonate (SB3-14). The integration of SB3-14 to the polyelectrolyte active layer dramatically enhanced the water permeability of the low-pressure nanofiltration (LNF) membrane without compromising the rejection of humic acid (HA). Specifically, the LNF membrane with intercalation of zwitterionic surfactant self-assemblies achieved a water permeability of up to 131 L $m^{-2}$ $h^{-1}$ $bar^{-1}$ and an HA rejection over 99%. In addition, the intercalation of SB3-14 surfactants also made the LNF membrane significantly smoother and less prone to fouling in long-term LNF operation, leading to higher water flux and HA rejection when the LNF process reached a steady state.

## 1. Introduction

Nanofiltration (NF) has received increasing interests in research and development in recent years due to its strong potential as a cost-effect approach for addressing emerging water treatment needs in the face of growing water scarcity and more stringent regulation [1–5]. NF membranes are generally classified into two categories based on its pore sizes: dense NF (DNF) membranes and low-pressure (or loose) NF (LNF) membranes. Dense NF membranes are capable of rejecting multivalent ions to a great extent. The applications of DNF include, but are not limited to, desalination of brackish groundwater [6], water softening [7,8] and wastewater reuse [9]. LNF membranes, on the other hand, refer to membranes with pore sizes between DNF membranes and ultrafiltration (UF) membranes. LNF has unique niches of applications. They can remove small organic molecules (e.g. dyes, or natural organic matter) that cannot be removed effectively by typical UF membranes, and at the same time have much higher water permeability and much lower pressure requirement than DNF or reverse osmosis that removes ionic species [9–11]. These characteristics enable LNF for highly efficient separation of organic molecules from feed water, which has a wide range of applications for water supply and wastewater reuse. Previous studies have shown LNF to be effective in removing hormones [12], pesticides [13], persistent organic pollutants (POPs) [14], pharmaceutically active compounds [15], and natural organic matters (NOMs) from surface water or ground water [16]. In particular, removal of NOMs by LNF can be a cost-effective approach as reverse osmosis pretreatment to reduce fouling [17], or as disinfection pretreatment to mitigate the formation of disinfection byproducts [18].

The cost-effective application of LNF requires LNF membranes with high perm-selectivity and fouling resistance. Significant enhancement of water permeability of NF membranes without sacrificing its selectivity can potentially result in a dramatic reduction of the required membrane area and energy consumption, which will translate to considerable cost reduction [19]. Toward this goal, various approaches have been explored for enhancing the water permeability of LNF membranes [19–21]. The specific approach for performance enhancement is strongly dependent on the fabrication method. One important and widely investigated fabrication method is layer-by-layer (LbL) deposition of polyelectrolytes [22–24]. In this method, polyanions and polycations are deposited alternately onto a substrate membrane (typically a UF membrane) to form a polyelectrolyte multi-layer that serves as the active layer for molecular separation [25,26]. This method has several unique advantages, such as high controllability of the active layer composition and properties, good fouling resistance, and possibility of

* Corresponding author. Department of Civil and Environmental Engineering, Vanderbilt University, Nashville, TN, 37235, United States.
*E-mail address:* shihong.lin@vanderbilt.edu (S. Lin).

https://doi.org/10.1016/j.memsci.2019.117726
Received 14 October 2019; Received in revised form 25 November 2019; Accepted 5 December 2019
Available online 6 December 2019

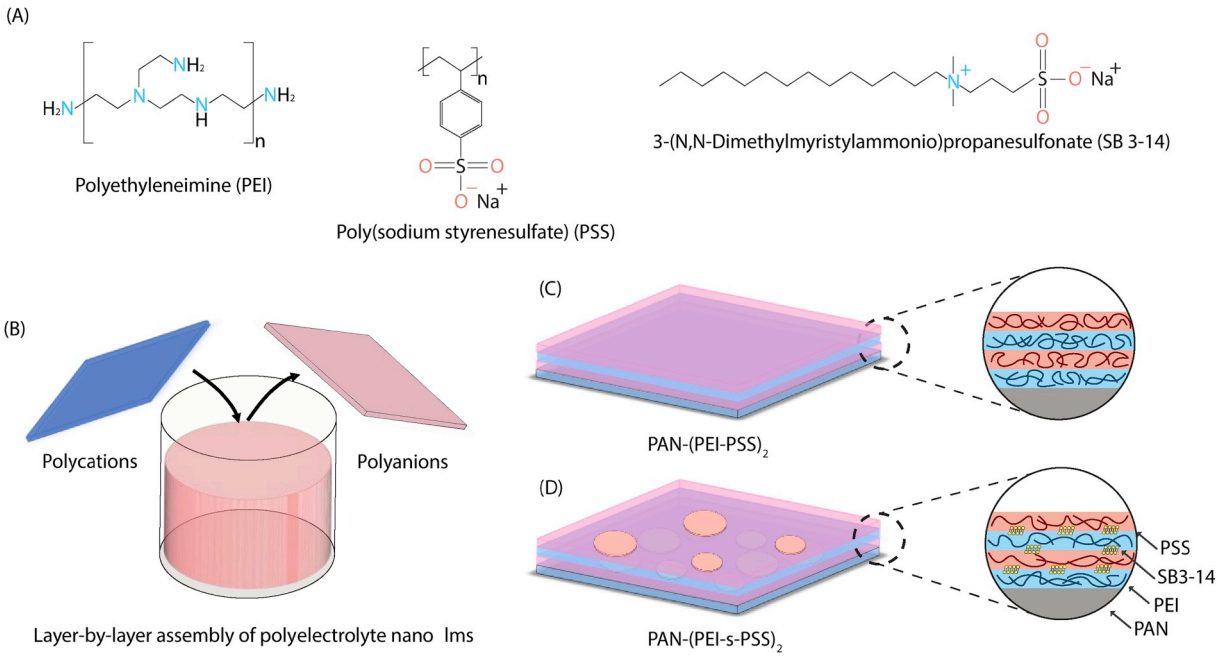


**Fig. 1.** (A) Chemical structures of the two polyelectrolytes (PEI and PSS) and the zwitterionic surfactant (SB 3–14) used to prepare the LNF membranes based on LbL deposition of polyelectrolyte. (B) Preparation of LbL polyelectrolyte membranes via the dip-coating method. (C) Schematic of a four-layer $(PEI\text{-}PSS)_2$ LNF membrane. (D) Schematic of a seven-layer $(PEI\text{-}s\text{-}PSS)_2$ LNF membrane.

using aqueous solution only in the fabrication process [23,27–30].

The key performance parameters of an LNF membrane include water permeability and rejection of target solutes. With the method of LbL deposition of polyelectrolytes, these performance parameters can be adjusted by altering the concentration of the polyelectrolytes [31], the deposition duration [31], and the solution chemistry [32,33]. Previous approaches for enhancing the perm-selectivity of membranes fabricated using LbL deposition of polyelectrolyte include tailoring the active layer thickness via adding salts or tuning the pH during polyelectrolyte deposition to either improve ion separation or reduce the hydraulic resistance for water transport [34–36], enhancing the surface hydrophilicity via surface modification and crosslinking [24,28], and incorporating novel 2D materials such as graphene and carbon nanotubes to construct water channels [37,38]. However, LNF membranes with higher water permeability typically also have compromised rejection of the target solutes, which is widely recognized as the intrinsic tradeoff of perm-selectivity for semi-permeable membranes [39,40].

Here, we report a novel approach for dramatically enhancing the perm-selectivity and fouling resistance of LNF membranes fabricated using LbL deposition of polyelectrolyte for filtering humic acid (HA)—a representative species of NOMs found in natural water. The reference LbL membrane is fabricated by depositing polyethyleneimine (PEI) and polystyrenesulfonate (PSS) alternately onto a polyacrylonitrile ultrafiltration membrane as the substrate. The main innovation of the reported approach is the intercalation of zwitterionic surfactants (SB3-14) self-assemblies between the PSS and the PEI layers which drastically improves the water permeability of LNF membranes by several folds without compromising its selectivity. We fabricate and characterize the polyelectrolyte membranes with and without SB3-14, and systematically compare their performance in LNF in terms of water permeability, organic rejection, and fouling resistance.

## 2. Materials and methods

### 2.1. Materials and chemicals

Polyacrylonitrile ultrafiltration (PAN, UF) membrane (MWCO = 50 kDa, GE Healthcare Life Science) was used as the substrate for fabricating the NF membrane. Polyethylenimine (PEI, Mw = 750 kDa), Polystyrene sulfonate (PSS, 10 000 kDa), 3-(*N, N*-Dimethylmyristylammonio) propanesulfonate (SB3-14, ≥99%), (3-Aminopropyl) triethoxysilane (APTES) (99%), hydrochloric acid (HCl, ACS reagent, 37%), sodium hydroxide (NaOH, Bioxtra, ≥ 98%), Humic acid (HA), methyl blue (MB, Mw = 799.8), $Na_2SO_4$ (≥99%), $MgSO_4$ (≥99.5%), $MgCl_2$ (≥99.99%), NaCl (≥99%) were purchased from Sigma-Aldrich (St. Louis, MO US). All chemicals were used as received without purification. Deionized water (Millipore, US) was used to prepare polyelectrolyte solution and surfactant solution.

### 2.2. Fabrication of $(PEI\text{-}PSS)_n$ and $(PEI\text{-}s\text{-}PSS)_n$ LNF membrane

The reference membrane $(PEI\text{-}PSS)_n$ low-pressure nanofiltration (LNF) membrane was prepared by depositing PEI and PSS alternately on a PAN ultrafiltration (UF) membrane (the chemical structures of PEI and PSS are shown in Fig. 1A). The PAN UF membrane was first treated with 2 mol $L^{-1}$ NaOH solution for 30 min to acquire negative surface charge, then immersed into DI water to remove excess NaOH, and dried in the oven at 30 °C over night before use. The freshly hydrolyzed PAN membrane was exposed to the polycation solution (1 g $L^{-1}$ PEI) for 30 min, rinsed with DI water, and then exposed to a polyanion solution (2 g $L^{-1}$ PSS) for another 30 min, and finally rinsed with DI water. The resulting membrane is referred as the $(PEI\text{-}PSS)_1$ with the subscript "1" representing one PEI-PSS bilayer (Fig. 1B). The same procedure was repeated to form additional bilayers, forming $(PEI\text{-}PSS)_2$ and $(PEI\text{-}PSS)_3$ (Fig. 1C for $(PEI\text{-}PSS)_2$). Regardless of the number of bilayers, these $(PEI\text{-}PSS)_n$ membranes are all referred to as the reference membranes.

The preparation of polyelectrolyte multilayer LNF membrane with surfactant intercalation followed a similar procedure as that for preparing the reference membranes except for an additional step of surfactant intercalation between the polycation and polyanion layers (Fig. 1D). Specifically, after each deposition of polycations (PEI) or polyanions (PSS) layer, the membrane was immersed into an aqueous solution of zwitterionic surfactant, SB3-14, for 30 min. The resulting polyelectrolyte multilayer membranes with intercalated surfactants are

referred to as $(PEI\text{-}s\text{-}PSS)_n$, with the subscript "n" representing the number of "PEI-s-PSS" tri-layers. We note that SB3-14 was also inserted between two adjacent "PEI-s-PSS" tri-layers and that PSS was also used as the final layer of the membranes for performance testing. Polyanion PSS was chosen as the material for the capping layer because most natural contaminants are negatively charged and are thus more effectively rejected by a membrane with a negatively charged surface.

### 2.3. Membrane characterization

The $\zeta$-potentials of the $(PEI\text{-}PSS)_n$ and $(PEI\text{-}s\text{-}PSS)_n$ membranes with different numbers of bi-layers or tri-layers were measured using a streaming potential analyzer (SurPASS electrokinetic analyzer, Anton Paar, Ashland, VA) with an adjusting gap cell and 1 mM KCl solution as the background electrolyte. The surface hydrophilicity of the $(PEI\text{-}PSS)_n$ and $(PEI\text{-}s\text{-}PSS)_n$ membranes at different deposition steps was quantified using in-air water contact angle measured with an optical tensiometer (Theta Lite, Biolin Scientific). The surface morphology of the $(PEI\text{-}PSS)_n$ and $(PEI\text{-}s\text{-}PSS)_n$ membranes was characterized with a high-resolution Zeiss Merlin scanning electron microscope (SEM) equipped with GEMINI II column with an accelerating voltage of 3 kV. Atomic force microscopy (AFM) was also employed to characterize the surface roughness of $(PEI\text{-}PSS)_n$ and $(PEI\text{-}s\text{-}PSS)_n$ membranes.

### 2.4. Characterization of surfactant self-assembly on a solid-water interface

Direct observation of SB3-14 self-assemblies on the polyelectrolyte active layer is challenging due to the intrinsic roughness of the polyelectrolyte coated UF membrane. Therefore, instead of using a UF membrane, we used a highly smooth substrate on which the morphology of SB3-14 self-assembly can be identified. Specifically, a molecularly smooth silicon (Si) wafer was first treated with a 0.1 M NaOH solution for 10 min and subsequently with 0.1 M $HNO_3$ solution for 10 min to acquire abundant surface hydroxyl groups. After being rinsed with water and dried with nitrogen, the treated Si substrate was then immersed in a toluene solution of 2.5 wt% aminopropyl trimethoxysilane (APTES) for 4 h with the headspace filled with nitrogen. This step of APTES coating was intended to impart positive charge to the Si substrate. The coated Si substrate was cleaned with toluene to remove excess APTES, dried under nitrogen, and then immersed in the aqueous solution of 0.4 mM SB3-14 (1 critical micelle concentration, CMC) for 30 min to obtain the self-assemblies of SB3-14 on the APTES-coated Si surface. The surface morphology of resulting Si substrate with SB3-14 adsorption was characterized by AFM.

### 2.5. NF performance evaluation

Nanofiltration performance of the $(PEI\text{-}PSS)_n$ and $(PEI\text{-}s\text{-}PSS)_n$ LNF membranes was evaluated using a cross-flow stainless steel filtration cell with an active membrane area of 7.1 $cm^2$. The pure water permeability of $(PEI\text{-}PSS)_n$ and $(PEI\text{-}s\text{-}PSS)_n$ membranes was evaluated using DI water before preforming any solute filtration. The cross-flow velocity was 10 L $h^{-1}$, the applied pressure was 2 bar and the temperature was kept at 25 °C. We evaluated the rejection of HA (10 mg $L^{-1}$) and methyl blue (500 mg $L^{-1}$), which are the primary species intended to be removed by the fabricated LNF membranes. However, the rejections of common salts with monovalent and divalent ions, including $Na_2SO_4$, $MgSO_4$, $MgCl_2$ and NaCl, were also evaluated. A concentration of 0.1 g $L^{-1}$ was used in all tests for measuring salt rejection. The concentrations of HA and methyl blue of the permeate and feed solution were determined using the UV–vis photometry (with calibration curves) at corresponding absorption wavelengths of 254 nm and 660 nm, respectively. The salt concentrations of the feed and permeate solutions were determined by measuring the electrical conductivity. All measurements were carried out after the system stabilized.

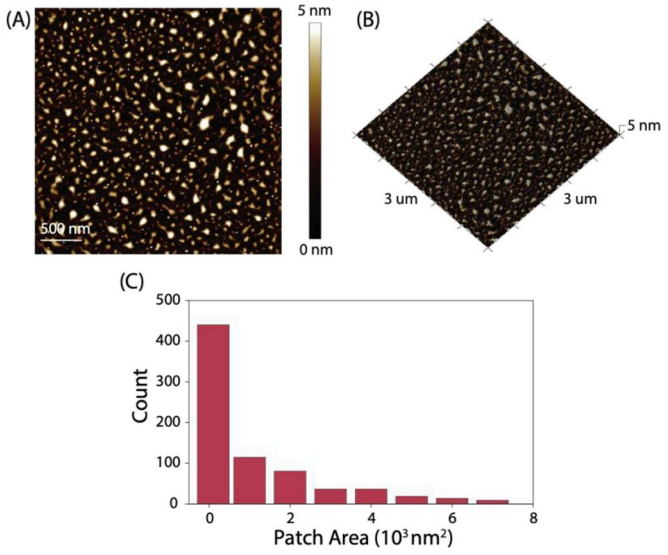


**Fig. 2.** (A and B) AFM topography and 3D height image of self-assembled SB3-14 patches on a smooth silicon wafer coated with APTES. (C) Size distribution of self-assembled SB3-14 patches on the silicon wafer obtained by analyzing Fig. 2A using Image-J. (For interpretation of the references to colour in this figure legend, the reader is referred to the Web version of this article.)

The pure water permeability of LNF membrane was calculated by weight measurement using the following equation:

$$PWP = \frac{J}{\Delta P} \tag{1}$$

where $PWP$ is the pure water permeability of LNF membrane (L $m^{-2}$ $h^{-1}$ $bar^{-1}$), where $J$ is the volumetric flux of water (L $m^{-2}$ $h^{-1}$), and $\Delta P$ was the applied pressure (bar), respectively. The rejection of solutes, $R$, is calculated using the following equation:

$$R = \left(1 - \frac{c_p}{c_f}\right) \times 100\% \tag{2}$$

where $c_p$ and $c_f$ are the solute concentration of permeate and feed solution, respectively.

### 2.6. Determination of pore size distribution and molecular weight cutoff (MWCO)

The pore size distributions of $(PEI\text{-}PSS)_n$ and $(PEI\text{-}s\text{-}PSS)_n$ LNF membranes were determined by fitting the rejection of a series of neutral organic compounds with increasing molecular weight. These neutral organic compounds include glucose (180 Da), sucrose (342 Da), raffinose (504 Da) and β-cyclodextrin (1135 Da). The concentration of the solutions containing each organic compound was 200 ppm and the applied pressure in the filtration experiments was 2 bar. The MWCO of the LNF membranes was defined as the molecular weight at which the rejection equals 90%. The pore size distribution is expressed as a probability density function (PDF) established based on the following assumption: (1) There is no steric or hydrodynamic interaction between these organic solutes and the membrane pores; (2) The mean pore size of the polyamide membrane equals the Stokes radius of the organic solute with a measured rejection of 50%; (3) The distribution of the membrane pore size is characterized by the geometric standard deviation of the PDF curve, which is the ratio between the Stokes radius with a rejection of 84.13% to that with a rejection of 50% [41].

$$\frac{dR(r_p)}{dr_p} = \frac{1}{r_p ln\sigma_p \sqrt{2\pi}} \exp\left[-\frac{(lnr_p - ln\mu_p)^2}{2(ln\sigma_p)^2}\right] \tag{3}$$

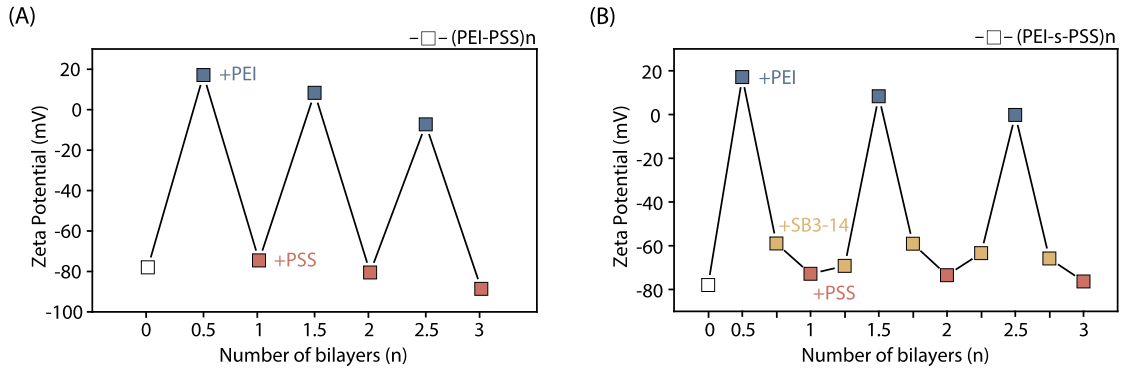


**Fig. 3.** Surface zeta potential of the LNF membrane in different steps of the LbL deposition process: (A) $(PEI\text{-}PSS)_n$ LNF membrane; (B) $(PEI\text{-}s\text{-}PSS)_n$ LNF membrane.

where $R(r_p)$ is the rejection of the organic solutes with a Stokes radius $r_p$, $\mu_p$ is the mean pore size, and $\sigma_p$ is the geometric standard deviation of the PDF curve.

## 3. Results and discussion

### 3.1. Self-assembly of zwitterionic surfactants on the water-solid interface

The SB3-14 surfactants self-assembled on a smooth Si wafer surface, forming patches with an average height of 5 nm (Fig. 2A). This average patch thickness is close to the thickness of SB3-14 micelles/bilayer measured using other characterization techniques [42–44]. The area of these patches varies from tens to thousands of $nm^2$ (Fig. 2B and C). The relatively small aspect ratio between the width and the height for most SB3-14 self-assemblies suggests that the self-assemblies are mostly micelles or micelle-sized bilayers, which is consistent with previous studies of adsorption of zwitterionic surfactants on hydrophilic silicon nitride or mica surfaces that reported micelle structure for the adsorbed aggregates [44,45]. In this case, however, large bilayers (i.e., "pancake" like structures) were also present according to the patch size statistics (Fig. 2C).

Due to the significantly larger intrinsic roughness of the substrate membrane as compared to the that of the SB3-14 self-assemblies, we cannot directly perform a similar characterization of the morphology of SB3-14 self-assemblies on a substrate membrane. However, the results from the AFM characterization of the SB3-14 self-assemblies on a smooth Si wafer surface provide insights into how SB3-14 possibly behaves when they adsorb onto a membrane substrate.

### 3.2. Surface property of surfactant-integrated polyelectrolyte multilayer LNF membrane

The deposition of PSS onto a PEI-coated surface and the deposition of PEI onto a PSS-coated surface are confirmed with the alternating signs of the zeta potentials of the $(PEI\text{-}PSS)_3$ membrane at different deposition steps (Fig. 3A). With a growing number of PEI-PSS layers, the PEI-coated surface became slightly less positive and the PSS-coated surface became slightly more negative. When constructing the $(PEI\text{-}s\text{-}PSS)_3$ membrane, the adsorption of the SB3-14 onto the PEI-coated surface appears to be much more effective than onto the PSS-coated membrane according to the corresponding changes of zeta potential (Fig. 3B). Specifically, the adsorption of SB3-14 consistently reversed the charge of the PEI-coated substrate to around −60 mV. Further adsorption of the PSS onto an SB3-14-coated PEI surface was confirmed by the additional reduction of zeta potential. However, such an additional reduction is relatively small compared to the reduction resulting from SB3-14 adsorption.

The unique chemical structure of a zwitterionic surfactant allows its adsorption onto both positively and negatively charged surfaces. In this case, SB3-14 can adsorb onto the negatively charged PSS surface because of the presence of the cationic quaternary ammonium. However, because the quaternary ammonium cations are located in the middle of the SB3-14 chains, the interaction between the cationic ammonium groups and the negatively charged PSS is hindered both sterically and electrostatically by the sulfonic groups at the end of the SB3-14 chains. Consequently, the change of zeta potential caused by the adsorption of SB3-14 onto PSS is dramatically smaller than that caused by the adsorption of SB3-14 onto PEI (Fig. 3B).

As the growth mechanism of polyelectrolyte multilayers is primarily driven by charge overcompensation and spatial redistribution [31,33], the reduction of surface charge density by the adsorption of zwitterionic surfactants decreases the degree of the subsequent adsorption of the oppositely charged polyelectrolyte. Therefore, the presence of SB3-14 self-assemblies leads to a thinner polyelectrolyte coating, which is beneficial for increasing membrane permeability as will be discussed later.

The NaOH-treated PAN substrate membrane became strongly

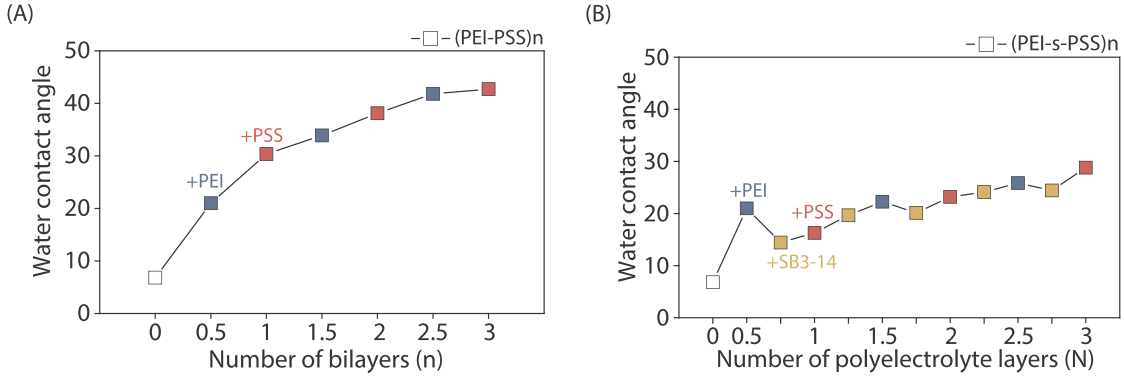


**Fig. 4.** Water contact angle of the LNF membrane in different steps of the LbL deposition process: (A) $(PEI\text{-}PSS)_n$ LNF membrane; (B) $(PEI\text{-}s\text{-}PSS)_n$ LNF membrane.

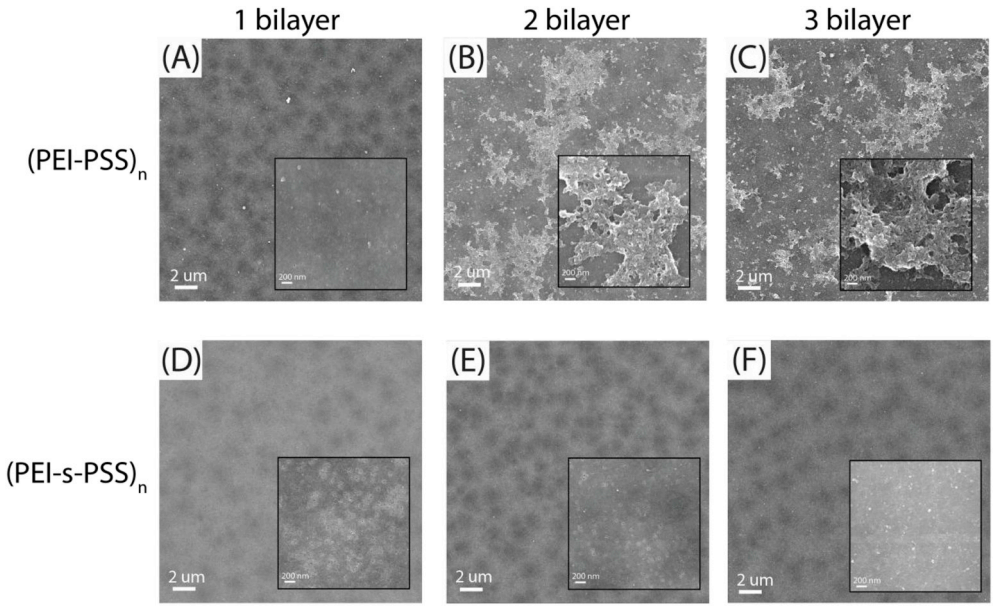


**Fig. 5.** Surface morphology of the LNF membrane in different steps of the LbL deposition process: (A, B and C) $(PEI\text{-}PSS)_n$ LNF membrane (D, E and F) $(PEI\text{-}s\text{-}PSS)_n$ LNF membrane.

hydrophilic with a water contact angle (WCA) lower than 10°. When fabricating the $(PEI\text{-}PSS)_n$ membrane, the adsorption of polyanion and polycation consistently increased the WCA, especially for the first few layers (Fig. 4A). The impact of SB3-14 addition is more complicated when fabricating the $(PEI\text{-}s\text{-}PSS)_n$ membrane. The adsorption of SB3-14 onto a PEI-coated surface decreased the WCA consistently, even though the WCA reduction becomes increasingly smaller with a growing number of layers (Fig. 4B). The reduction of WCA by the adsorption of the SB3-14 is additional indirect evidence that SB3-14 exists on the membrane substrate as bilayers instead of monolayers, as otherwise, the exposed hydrophobic tails in a monolayer would undoubtedly have increased the WCA. However, the adsorption of the SB3-14 onto a PSS-coated surface increased the WCA, possibly because the zwitterionic charged head of SB3-14 does not interact with water as strongly as the sulfonic group in the PSS. Comparing the WCA between the $(PEI\text{-}PSS)_n$ and $(PEI\text{-}s\text{-}PSS)_n$ membranes, the addition of SB3-14 makes the LNF membrane considerably more hydrophilic.

### 3.3. Morphology and surface roughness of $(PEI\text{-}s\text{-}PSS)_n$ LNF membrane

The surface morphology of the $(PEI\text{-}PSS)_n$ and $(PEI\text{-}s\text{-}PSS)_n$ LNF membranes with different numbers of polyelectrolyte active layers was characterized using SEM and AFM. For $(PEI\text{-}PSS)_n$ membrane, increasing the polyelectrolyte layers results in more heterogeneous surface morphology, i.e., the formation of self-assembled polyelectrolyte patches on the membrane surface (Fig. 5A–C). The increase of polyelectrolyte roughness was attributed to the so-called "nonmonotonic adsorption behavior" that occurs when strong polyelectrolytes adsorb onto a weakly charged polyelectrolyte surface [46–48]. If the degree of the ionization of the weak polyelectrolyte in the multilayers is below a critical charge density, the following adsorption of a fully charged polyelectrolyte will encounter a thermodynamic frustration. Specifically, the adsorption of PSS onto the PEI surface was carried out at pH of 7, where PEI (pka ~7) was approximately 50% ionized [49]. When the fully ionized polyelectrolyte (PSS) adsorbed onto the weakly ionized PEI surface, the enthalpic gain for the PSS chain to extend horizontally and maximize its contact with the substrate surface is insufficient to overcome the entropic penalty associated with this conformation [48]. Therefore, the absorbed PSS chains onto the PEI surface formed a large number of tails and loops, which increased the surface roughness. Such

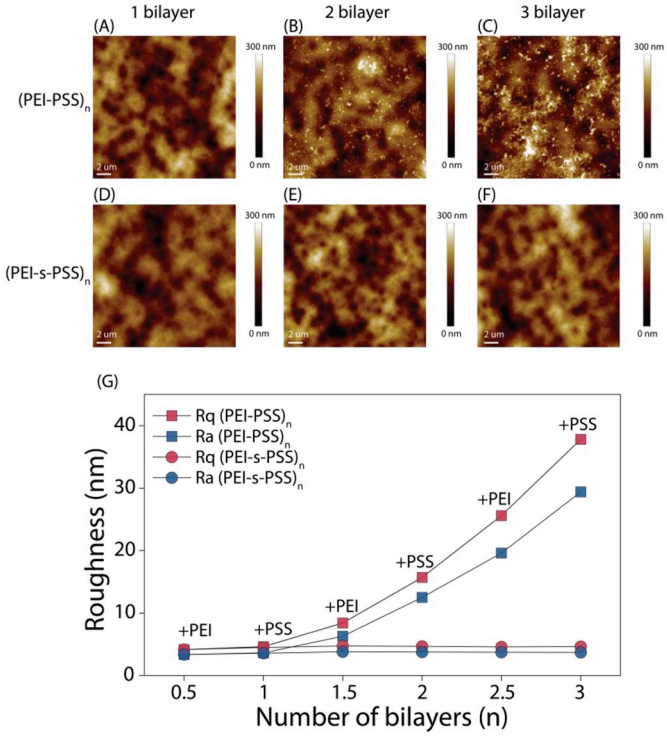


**Fig. 6.** Surface morphology of (A, B, C) $(PEI\text{-}PSS)_n$ LNF membranes and (D, E, F) $(PEI\text{-}s\text{-}PSS)_n$ LNF membranes. (G) Surface roughness of $(PEI\text{-}PSS)_n$ and $(PEI\text{-}s\text{-}PSS)_n$ LNF membranes in different steps of the LbL deposition process.

an effect of non-extended adsorption became growingly significant with increasing number of layers, as the positive charge of PEI continued to decrease as the number of layers increased [48].

The morphology of the $(PEI\text{-}s\text{-}PSS)_n$ membrane is dramatically different from that of the $(PEI\text{-}PSS)_n$ membrane. The integration of surfactants between the polycation and polyanion eliminates the surface heterogeneity. Specifically, the $(PEI\text{-}s\text{-}PSS)_n$ membrane surface is free of large heterogeneous patches observed on the surface of the $(PEI\text{-}PSS)_n$

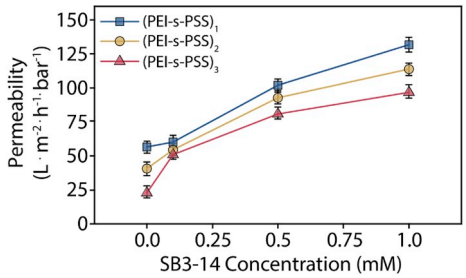


**Fig. 7.** Water permeability of the $(PEI\text{-}s\text{-}PSS)_n$ with different surfactant concentrations and different numbers of assembly layers. (Permeability data represents the average of three runs).

membrane (Fig. 5D–F). The morphological difference between the $(PEI\text{-}PSS)_n$ and $(PEI\text{-}s\text{-}PSS)_n$ membranes is further confirmed by comparing their respective AFM micrographs (Fig. 6A–F) from which the surface roughness was quantified (Fig. 6G). The roughness of the $(PEI\text{-}PSS)_n$ membrane increased rapidly as the number of polyelectrolyte layers increased, whereas the roughness of the $(PEI\text{-}s\text{-}PSS)_n$ membrane constantly remained low (Fig. 6G).

This dramatic effect of surfactant intercalation on smoothening the membrane formed via LBL of polyelectrolytes has not been documented in the literature. The zeta potentials at different steps of constructing the $(PEI\text{-}PSS)_n$ and $(PEI\text{-}s\text{-}PSS)_n$ membranes (Fig. 3) suggest that substantially less PSS adsorbed onto the $(PEI\text{-}s\text{-}PSS)_n$ membrane than onto the $(PEI\text{-}PSS)_n$ membrane. The likely explanation for this difference is the elimination of available adsorption sites on PEI by the patchy SB3-14 bilayers in constructing the $(PEI\text{-}s\text{-}PSS)_n$ membrane. Even though ammonium groups are also present in the SB3-14, the screening of the adjacent sulfonic groups renders the ammonium groups hardly available for PSS adsorption.

Let us compare the adsorption of PSS onto a PEI-coated surface, as in constructing a $(PEI\text{-}PSS)_n$ membrane, and onto a PEI-coated surface with adsorbed SB3-14, as in constructing a $(PEI\text{-}s\text{-}PSS)_n$ membrane. Because the PEI-coated surface is positively charged and has relatively abundant adsorption sites, the adsorption of PSS is fast, but the full extension of PSS along the PEI surface is prohibited by both conformational entropic penalty and steric hindrance (between neighboring PSS molecules). When the PEI-coated substrate is decorated with SB3-14, the surface is highly negative (Fig. 3B) and the uncoated adsorption sites on PEI become limited. Therefore, PSS adsorption is substantially slower due to the overall electrostatic repulsion, and successful adsorption can only occur if the orientation of the PSS chains happens to favor the extension of the PSS along the surface to maximize the contact between PSS and the distributed uncoated adsorption sites on PEI. The fact that a more compact PSS layer can form when the PSS adsorption is kinetically unfavorable is to a certain extent similar to the formation of more "compact" aggregates in reaction-limited aggregation, which has been well studied in colloidal physics [50,51] Specifically, reaction-limited aggregation is kinetically unfavorable, which in turn allows the primary particles to diffuse deeper into the center of porous aggregate, leading to the growth of aggregates with a higher fractal dimension.

### 3.4. *Pure water permeability of $(PEI\text{-}s\text{-}PSS)_n$ LNF membrane*

The intercalation of SB3-14 dramatically enhances the pure water permeability of the resulting $(PEI\text{-}s\text{-}PSS)_n$ LNF membranes (Fig. 7). The degree of permeability enhancement depends on the number of layers and the surfactant concentrations used in the intercalation step. In general, a higher SB3-14 concentration results in a more significant enhancement of water permeability, regardless of the number of polyelectrolyte layers. With a given SB3-14 concentration, the permeability decreased with a higher number of layers deposited. However, the relative (i.e., in terms of percentage) performance differences between membranes with the different number of polyelectrolyte layers are the most salient for $(PEI\text{-}PSS)_n$ membrane without any surfactant integration. In other words, the integration of surfactants does not only enhance the water permeability but also reduce the relative difference in water permeability between $(PEI\text{-}s\text{-}PSS)_n$ with different numbers of layers. Notably, using 1.0 mM of SB3-14 for intercalation improves the water permeability of $(PEI\text{-}PSS)_1$ and $(PEI\text{-}PSS)_3$ membranes by ~300% and ~500%, respectively.

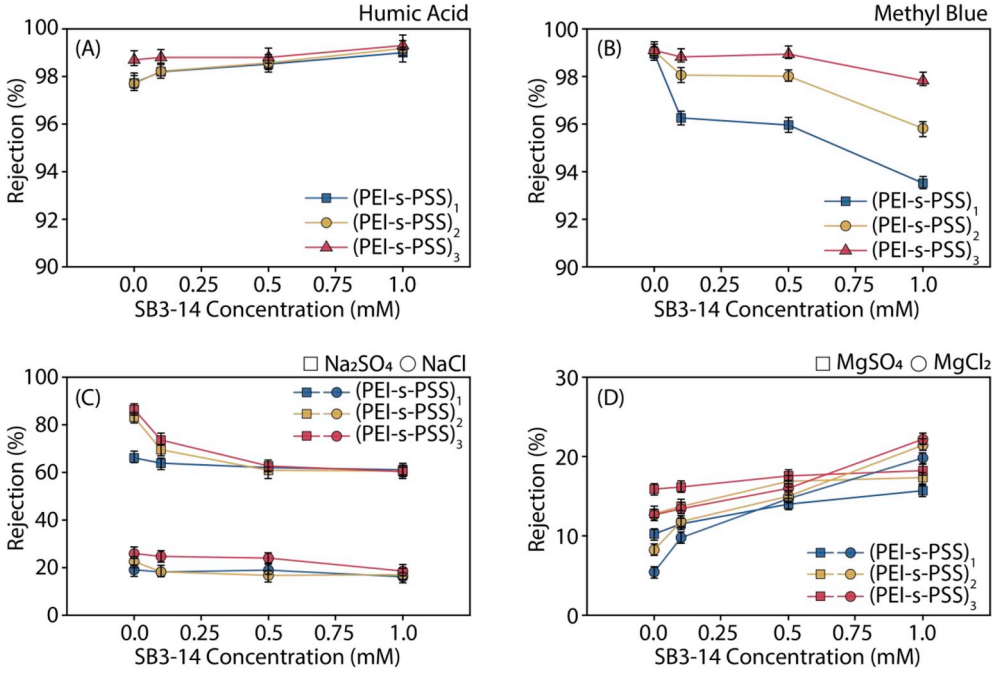


**Fig. 8.** Separation performance of the $(PEI\text{-}s\text{-}PSS)_n$ LNF membranes with different surfactant concentrations and number of assembly layers. (A) Humic acid (B) Methyl Blue (C) $Na_2SO_4$ and NaCl (D) $MgSO_4$ and $MgCl_2$ (rejection data represents the average of three runs). (For interpretation of the references to colour in this figure legend, the reader is referred to the Web version of this article.)

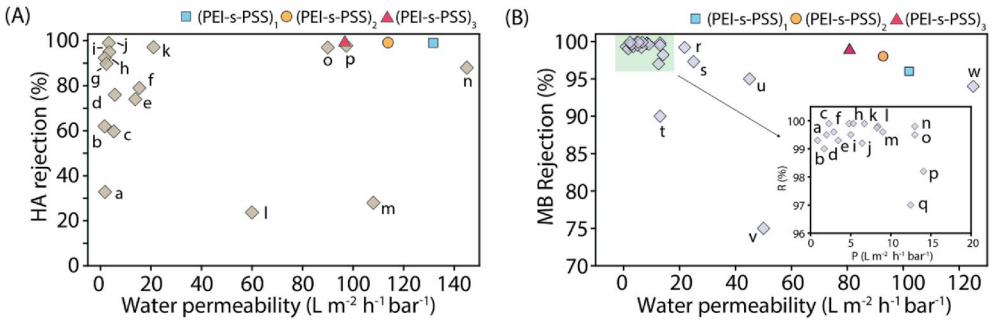


**Fig. 9.** (A) Comparison of water permeability and HA rejection of $(PEI\text{-}s\text{-}PSS)_n$ LNF membrane (SB3-14 concentration is 1 mM) with other NF membranes reported in the literature (a,b, [54]; c,f, [55]; d, [56]; e, [57]; g,h [58], i, [59]; j, [57]; k, [16]; l,m, [60]; n, [61]; o, [62]; p, [63]). (B) Comparison of water permeability and methyl blue rejection of $(PEI\text{-}s\text{-}PSS)_n$ LNF membrane (SB3-14 concentration is 0.5 mM) with other NF membranes reported in the literature (a [64]; b [65]; c,d,g,h [66]; e,o,p [30]; f [67]; i [68]; j [69]; k [70]; l, [71]; m,n [72]; q,s [73]; r [74]; t [21]; u [75]; v [76]; w [63]). (For interpretation of the references to colour in this figure legend, the reader is referred to the Web version of this article.)

### 3.5. Solute rejection of $(PEI\text{-}s\text{-}PSS)_n$ LNF membrane

The integration of zwitterionic surfactants did not only enhance the water permeability substantially but also increased the rejection of humic acid (Fig. 8A). In fact, as the concentration of SB3-14 in the intercalation step increased, the HA rejection of the $(PEI\text{-}s\text{-}PSS)_1$ membrane increased from 97% to 99%. We note that a higher rejection of HA does not necessarily mean the membrane is "less permeable" to HA because the rejection of a solute represents the relative permeability of a membrane to solute as compared to water. In this case, because the addition of SB3-14 enhances the water permeability by ~3 folds, as long as the permeability of HA does not increase by the same degree or more, the rejection of HA increases. A previous study on fabricating $(PEI\text{-}PSS)_n$ LNF membrane using similar compositions of PEI and PSS but without the surfactant intercalation reported an HA rejection of only 97% even with five layers of PEI and PSS [16]. The corresponding water permeability for that $(PEI\text{-}PSS)_5$ membrane was only ~ 12 L $m^{-2}$ $h^{-1}$ $bar^{-1}$, which is less than 1/10 of the water permeability of a $(PEI\text{-}s\text{-}PSS)_1$ LNF membrane fabricated in this work (~131 L $m^{-2}$ $h^{-1}$ $bar^{-1}$) even though the membrane reported in this work has an even higher HA rejection.

While the intercalation of SB3-14 is effective in maintaining, or even increasing, the HA rejection, it compromises the rejection of methyl blue which is a negatively charged dye molecule (Fig. 8B). For relatively small charged molecules (as compared to HA), the Donnan exclusion effect has an important contribution to the overall solute rejection [52,53]. Compared with the $(PEI\text{-}PSS)_n$ membranes, the $(PEI\text{-}s\text{-}PSS)_n$ membranes have less negative zeta potential (Fig. 3B), possibly due to reduced adsorption of the PSS. Consequently, the Donnan exclusion of negatively charged methyl blue molecules is also weaker. However, because the differences in zeta potential between $(PEI\text{-}PSS)_n$ and $(PEI\text{-}s\text{-}PSS)_n$ are relatively small, we also speculate that the zwitterionic group on SB3-14 is ineffective in repelling methyl blue molecules due to the co-existence of cationic and anionic moieties near each other, even though the overall contribution of SB3-14 to surface potential is negative according to Fig. 3B. Additionaly, the intercalation of SB3-14 also increased the MWCO and the pore size of $(PEI\text{-}PSS)_n$ LNF membrane (see Fig. A1 in Appendix). Despite the negative impact of SB3-14 intercalation on the rejection of methyl blue, the absolute rejection of methyl blue still exceeds 93% in all cases. For membranes with three layers, integrating SB3-14 at a concentration of 1 mM only reduced the methyl blue rejection of ~99% for $(PEI\text{-}PSS)_3$–~98% for $(PEI\text{-}s\text{-}PSS)_3$—a very small compromise as compared to the tremendous gain in water flux.

The salt rejection of the $(PEI\text{-}s\text{-}PSS)_n$ LNF membranes was also evaluated, even though salt rejection is expectedly low for any LNF membrane. Specifically, the intercalation of SB3-14 reduced the rejection of $Na_2SO_4$, especially for membranes with two and three layers (Fig. 8C). When the SB3-14 concentration exceeds 0.5 mM, the $Na_2SO_4$ rejection is consistently ~60% regardless of the number of layers. In comparison, the integration of SB3-14 does not seem to have major impact on NaCl rejection. The rejection of NaCl is consistently low (~20%) regardless of the number of layers and the presence (and concentration) of SB3-14. Lastly, the integration of SB3-14 seems to enhance the rejection of $Mg^{2+}$ salt, even though the rejection can barely exceed 20% in all cases. It is well known that a negatively charged membrane is better in rejecting salts with multivalent anions (e.g., $Na_2SO_4$) than in rejecting salts with multivalent cations (e.g., $MgCl_2$), which is attributable to the fact that Donnan exclusion is a major rejection mechanism. The fact that the integration of SB3-14 undermines the rejection of $Na_2SO_4$ but improves the rejection of $MgCl_2$ is additional evidence that the presence of the SB3-14 bilayers reduces electrostatic interaction with solutes as compared to a PSS surface without surfactant intercalation.

### 3.6. Overall performance of $(PEI\text{-}s\text{-}PSS)_n$ membrane versus the state-of-the-art

As discussed in sections 3.4 and 3.5, the intercalation of SB3-14 dramatically enhances the water permeability of the LNF membrane without sacrificing its HA rejection. The $(PEI\text{-}s\text{-}PSS)_n$ membranes have exceptional performance not only just compared to the reference $(PEI\text{-}PSS)_n$ membranes but also compared to the state-of-the-art according to literature (Fig. 9A). Only two membranes reported in previous work could achieve a water permeability above 40 L $m^{-2}$ $h^{-1}$ $bar^{-1}$ while maintaining an HA rejection beyond 90% ("o" and "p" in Fig. 9). However, the $(PEI\text{-}s\text{-}PSS)_1$ membrane attains an exceptional water permeability of ~131 L $m^{-2}$ $h^{-1}$ $bar^{-1}$ and an outstanding HA rejection of 99%, far exceeding the state-of-the-art performance of LNF membranes for filtering HA solutions. The same conclusion can be drawn when comparing the rejection of methyl blue of $(PEI\text{-}s\text{-}PSS)_n$ membranes with the NF membranes reported in the literature (Fig. 9B). Although the intercalation of SB3-14 slight induces a trade-off of the membrane permeability and its rejection of methyl blue, the 3-bilayer $(PEI\text{-}s\text{-}PSS)_n$ membrane still yields a high rejection of 99% while maintaining the water permeability of 82 L $m^{-2}$ $h^{-1}$ $bar^{-1}$, which is collectively superior than state-of-the-art NF membranes reported in the literature.

### 3.7. Reduced fouling of the $(PEI\text{-}s\text{-}PSS)_n$ LNF membranes

It is widely recognized in the literature that membranes that are smoother and more hydrophilic are less prone to fouling [77–81]. Compared with the $(PEI\text{-}PSS)_3$ membrane, the $(PEI\text{-}s\text{-}PSS)_3$ LNF membrane was dramatically smoother (Fig. 5) and slightly more hydrophilic (Fig. 4). Consequently, the $(PEI\text{-}s\text{-}PSS)_3$ LNF membrane was substantially more fouling resistant than the $(PEI\text{-}PSS)_3$ LNF membrane in long-term filtration experiments with HA as the feed solution (Fig. 10). Not only the initial flux decline was much slower with the $(PEI\text{-}s\text{-}PSS)_3$ LNF membrane (Fig. 10A and B), but its normalized flux at steady state (i.e., no more flux decline) was also considerably higher than that with

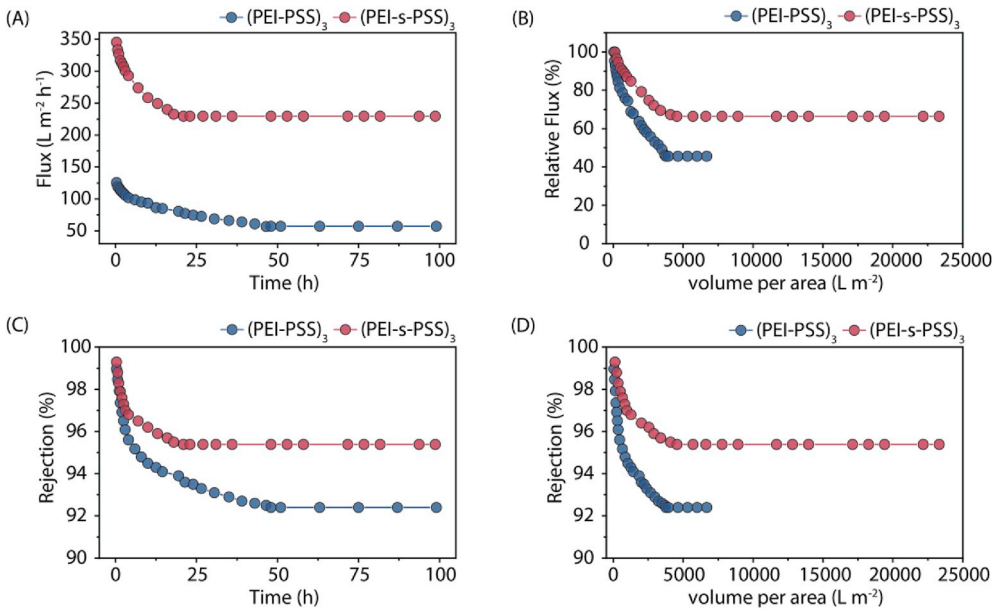


**Fig. 10.** (A) absolute flux as a function of time; (B) normalized flux as a function of permeate volume per membrane area; (C) HA rejection as a function of time; (D) HA rejection as a function of permeate volume per membrane area. In all panels, blue and red symbols represent data obtained using $(PEI-PSS)_3$ and $(PEI-s-PSS)_3$ membranes, respectively. (For interpretation of the references to colour in this figure legend, the reader is referred to the Web version of this article.)

the $(PEI-PSS)_3$ LNF membrane. Specifically, ~67% and ~45% of the initial fluxes were maintained at steady state with the $(PEI-s-PSS)_3$ and $(PEI-PSS)_3$ LNF membranes, respectively (Fig. 10B). The advantage of $(PEI-s-PSS)_3$ over $(PEI-PSS)_3$ is all the more salient if we consider the fact that the initial flux of the former is two to three folds of the later (Fig. 10A). The steady-state water flux for the $(PEI-s-PSS)_3$ membrane was 230 L $m^{-2}$ $h^{-1}$, whereas that for the $(PEI-PSS)_3$ membrane was only 57.2 L $m^{-2}$ $h^{-1}$.

We have shown in Section 3.5 that the integration of SB3-14 did not compromise, but even slightly improved, the HA rejection of the $(PEI-PSS)_n$ LNF membrane. When both membranes were subject to long-term filtration of an HA solution, an appreciable drop of HA rejection was observed for both membranes (Fig. 10C and D). Interestingly, the drop of rejection synchronized with the flux decline and reached a steady state (i.e., no more drop of rejection) when ~ 4,500 L and 3,700 L of feed water was filtered through 1 $m^2$ of $(PEI-s-PSS)_3$ and $(PEI-PSS)_3$ LNF membranes, respectively (Fig. 10D). As discussed in section 3.5, rejection is not only dependent on how permeable a membrane is to a specific solute but dependent on the water permeability. The synchrony between the changes of flux and HA rejection suggests that the reduction of HA rejection is primarily attributable to flux decline. Because the $(PEI-PSS)_3$ LNF membrane was subject to a larger percent of flux decline as compared to the $(PEI-s-PSS)_3$ membrane, it also suffered a more substantial reduction in HA rejection. Specifically, the HA rejection for $(PEI-PSS)_3$ and $(PEI-s-PSS)_3$ membranes dropped from ~99% to 92.2% and 95.5%, respectively, when filtration reached steady-state. Overall, the results in Fig. 10 suggest that the $(PEI-s-PSS)_3$ is systematically better than $(PEI-PSS)_3$ in long-term filtration of an HA feed solution, demonstrating slower flux decline, higher steady-state flux, and higher steady-state HA rejection.

## 4. Conclusion

We show in this study the effectiveness of using SB3-14 intercalation to dramatically improve the performance of LNF membranes formed via LbL deposition of PSS and PEI. The presence of SB3-14 self-assemblies resulted in smoother and more permeable LNF membranes. The resulting $(PEI-s-PSS)_n$ membrane achieved an outstanding water permeability of 131 L $m^{-2}$ $h^{-1}$ $bar^{-1}$ while maintaining an exceptional rejection of HA (99%). Compared to the reference $(PEI-PSS)_3$ membrane, the performance of the $(PEI-s-PSS)_3$ was also much more stable in long-term LNF operation as indicated by not only substantially less decline of normalized flux but also less decline in HA rejection. We attribute these remarkable improvements in performance and long-term stability to the unique active layer structure imparted by the integration of the SB3-14 self-assemblies. We believe that this strategy of surfactant intercalation is universally applicable for enhancing LNF membrane formed via LbL deposition of polyelectrolytes.

## Declaration of competing interest

The authors declare that they have no known competing financial interests or personal relationships that could have appeared to influence the work reported in this paper.

## CRediT authorship contribution statement

**Yuanzhe Liang:** Data curation, Investigation, Methodology, Visualization, Writing - original draft. **Shihong Lin:** Data curation, Investigation, Methodology, Conceptualization, Writing - review & editing.

## Acknowledgment

The authors are thankful for the support from the Desalination and Water Purification Research Program of the US Bureau of Reclamation via agreement R18AC00110.

## Appendix A. Supplementary data

Supplementary data to this article can be found online at https://doi.org/10.1016/j.memsci.2019.117726.

## References

[1] R.J. Petersen, Composite reverse osmosis and nanofiltration membranes, J. Membr. Sci. 83 (1993) 81–150, https://doi.org/10.1016/0376-7388(93)80014-O.
[2] A.W. Mohammad, Y.H. Teow, W.L. Ang, Y.T. Chung, D.L. Oatley-Radcliffe, N. Hilal, Nanofiltration membranes review: recent advances and future prospects, Desalination 356 (2015) 226–254, https://doi.org/10.1016/j.desal.2014.10.043.

[3] N. Hilal, N.A. Darwish, A.W. Mohammad, M.A. Arabi, A comprehensive review of nanofiltration membranes : treatment , pretreatment , modelling , and atomic force microscopy 170 (2004) 281–308, https://doi.org/10.1016/j.desal.2004.01.007.
[4] P.H. Gleick, Global freshwater resources: soft-path solutions for the 21st century, Science 302 (2003) 1524–1528, 80.
[5] M.M. Mekonnen, A.Y. Hoekstra, Four billion people facing severe water scarcity, Sci. Adv. 2 (2016), e1500323.
[6] C.M. Galanakis, G. Fountoulis, V. Gekas, Nanofiltration of brackish groundwater by using a polypiperazine membrane, Desalination 286 (2012) 277–284.
[7] W. Fang, L. Shi, R. Wang, Mixed polyamide-based composite nanofiltration hollow fiber membranes with improved low-pressure water softening capability, J. Membr. Sci. 468 (2014) 52–61.
[8] Z. Wang, Z. Wang, S. Lin, H. Jin, S. Gao, Y. Zhu, J. Jin, Nanoparticle-templated nanofiltration membranes for ultrahigh performance desalination, Nat. Commun. 9 (2018) 1–36, https://doi.org/10.1038/s41467-018-04467-3.
[9] C. Tang, V. Chen, Nanofiltration of textile wastewater for water reuse, Desalination 143 (2002) 11–20.
[10] J. Lin, W. Ye, H. Zeng, H. Yang, J. Shen, S. Darvishmanesh, P. Luis, A. Sotto, B. Van der Bruggen, Fractionation of direct dyes and salts in aqueous solution using loose nanofiltration membranes, J. Membr. Sci. 477 (2015) 183–193.
[11] J. Zhu, M. Tian, J. Hou, J. Wang, J. Lin, Y. Zhang, J. Liu, B. Van der Bruggen, Surface zwitterionic functionalized graphene oxide for a novel loose nanofiltration membrane, J. Mater. Chem. A. 4 (2016) 1980–1990.
[12] L.D. Nghiem, A.I. Schäfer, M. Elimelech, Removal of natural hormones by nanofiltration membranes: measurement, modeling, and mechanisms, Environ. Sci. Technol. 38 (2004) 1888–1896.
[13] K. Košutić, L. Furač, L. Sipos, B. Kunst, Removal of arsenic and pesticides from drinking water by nanofiltration membranes, Separ. Purif. Technol. 42 (2005) 137–144.
[14] A. Verliefde, E. Cornelissen, G. Amy, B. Van der Bruggen, H. Van Dijk, Priority organic micropollutants in water sources in Flanders and The Netherlands and assessment of removal possibilities with nanofiltration, Environ. Pollut. 146 (2007) 281–289.
[15] L.D. Nghiem, A.I. Schäfer, M. Elimelech, Pharmaceutical retention mechanisms by nanofiltration membranes, Environ. Sci. Technol. 39 (2005) 7698–7705.
[16] L. Shan, H. Guo, Z. Qin, N. Wang, S. Ji, G. Zhang, Z. Zhang, Covalent crosslinked polyelectrolyte complex membrane with high negative charges towards anti-natural organic matter fouling nanofiltration, RSC Adv. 5 (2015) 11515–11523.
[17] S. Gur-Reznik, I. Katz, C.G. Dosoretz, Removal of dissolved organic matter by granular-activated carbon adsorption as a pretreatment to reverse osmosis of membrane bioreactor effluents, Water Res. 42 (2008) 1595–1605.
[18] J.S. Taylor, C.R. Reiss, P.S. Jones, K.E. Morris, T.L. Lyn, Reduction of Disinfection By-Product Precursors by Nanofiltration, 1992.
[19] A.I. Schäfer, A.G. Fane, T.D. Waite, Cost factors and chemical pretreatment effects in the membrane filtration of waters containing natural organic matter, Water Res. 35 (2001) 1509–1517.
[20] J. Zhu, M. Tian, Y. Zhang, H. Zhang, J. Liu, Fabrication of a novel "loose" nanofiltration membrane by facile blending with Chitosan–Montmorillonite nanosheets for dyes purification, Chem. Eng. J. 265 (2015) 184–193.
[21] L. Yu, Y. Zhang, Y. Wang, H. Zhang, J. Liu, High flux, positively charged loose nanofiltration membrane by blending with poly (ionic liquid) brushes grafted silica spheres, J. Hazard Mater. 287 (2015) 373–383.
[22] J. Zhu, J. Wang, A.A. Uliana, M. Tian, Y. Zhang, Y. Zhang, A. Volodin, K. Simoens, S. Yuan, J. Li, Mussel-inspired architecture of high-flux loose nanofiltration membrane functionalized with antibacterial reduced graphene oxide–copper nanocomposites, ACS Appl. Mater. Interfaces 9 (2017) 28990–29001.
[23] W. Jin, A. Toutianoush, B. Tieke, Use of polyelectrolyte layer-by-layer assemblies as nanofiltration and reverse osmosis membranes, Langmuir 19 (2003) 2550–2553, https://doi.org/10.1021/la020926f.
[24] C. Liu, L. Shi, R. Wang, Crosslinked layer-by-layer polyelectrolyte nanofiltration hollow fiber membrane for low-pressure water softening with the presence of SO42− in feed water, J. Membr. Sci. 486 (2015) 169–176.
[25] B.W. Stanton, J.J. Harris, M.D. Miller, M.L. Bruening, Ultrathin, multilayered polyelectrolyte films as nanofiltration membranes, Langmuir 19 (2003) 7038–7042.
[26] R. Malaisamy, M.L. Bruening, High-flux nanofiltration membranes prepared by adsorption of multilayer polyelectrolyte membranes on polymeric supports, Langmuir 21 (2005) 10587–10592.
[27] K.L. Cho, A.J. Hill, F. Caruso, S.E. Kentish, Chlorine resistant glutaraldehyde crosslinked polyelectrolyte multilayer membranes for desalination, Adv. Mater. 27 (2015) 2791–2796.
[28] T. Ishigami, K. Amano, A. Fujii, Y. Ohmukai, E. Kamio, T. Maruyama, H. Matsuyama, Fouling reduction of reverse osmosis membrane by surface modification via layer-by-layer assembly, Separ. Purif. Technol. 99 (2012) 1–7.
[29] C. Ba, D.A. Ladner, J. Economy, Using polyelectrolyte coatings to improve fouling resistance of a positively charged nanofiltration membrane, J. Membr. Sci. 347 (2010) 250–259, https://doi.org/10.1016/J.MEMSCI.2009.10.031.
[30] L. Wang, N. Wang, J. Li, J. Li, W. Bian, S. Ji, Layer-by-layer self-assembly of polycation/GO nanofiltration membrane with enhanced stability and fouling resistance, Separ. Purif. Technol. 160 (2016) 123–131.
[31] S.T. Dubas, J.B. Schlenoff, Factors controlling the growth of polyelectrolyte multilayers, Macromolecules 32 (1999) 8153–8160, https://doi.org/10.1021/ma981927a.
[32] S.S. Shiratori, M.F. Rubner, pH-dependent thickness behavior of sequentially adsorbed layers of weak polyelectrolytes, Macromolecules 33 (2000) 4213–4219, https://doi.org/10.1021/ma991645q.
[33] J.B. Schlenoff, S.T. Dubas, Mechanism of polyelectrolyte multilayer growth: charge overcompensation and distribution, Macromolecules 34 (2001) 592–598, https://doi.org/10.1021/ma0003093.
[34] L. Krasemann, B. Tieke, Selective ion transport across self-assembled alternating multilayers of cationic and anionic polyelectrolytes, Langmuir 16 (2000) 287–290.
[35] R.M. DuChanois, R. Epsztein, J.A. Trivedi, M. Elimelech, Controlling pore structure of polyelectrolyte multilayer nanofiltration membranes by tuning polyelectrolyte-salt interactions, J. Membr. Sci. 581 (2019) 413–420, https://doi.org/10.1016/j.memsci.2019.03.077.
[36] Y. Liu, G.Q. Chen, X. Yang, H. Deng, Preparation of layer-by-layer nanofiltration membranes by dynamic deposition and crosslinking, Membranes 9 (2019), https://doi.org/10.3390/membranes9020020.
[37] M. Hu, B. Mi, Layer-by-layer assembly of graphene oxide membranes via electrostatic interaction, J. Membr. Sci. 469 (2014) 80–87.
[38] F.-Y. Zhao, Q.-F. An, Y.-L. Ji, C.-J. Gao, A novel type of polyelectrolyte complex/MWCNT hybrid nanofiltration membranes for water softening, J. Membr. Sci. 492 (2015) 412–421.
[39] H.B. Park, J. Kamcev, L.M. Robeson, M. Elimelech, B.D. Freeman, Maximizing the right stuff: the trade-off between membrane permeability and selectivity, Science 80– (2017) 356, eaab0530.
[40] G.M. Geise, H.B. Park, A.C. Sagle, B.D. Freeman, J.E. McGrath, Water permeability and water/salt selectivity tradeoff in polymers for desalination, J. Membr. Sci. 369 (2011) 130–138.
[41] G.E. Chen, Y.J. Liu, Z.L. Xu, Y.J. Tang, H.H. Huang, L. Sun, Fabrication and characterization of a novel nanofiltration membrane by the interfacial polymerization of 1,4-diaminocyclohexane (DCH) and trimesoyl chloride (TMC), RSC Adv. 5 (2015) 40742–40752, https://doi.org/10.1039/c5ra02560e.
[42] C. Tanford, Micelle shape and size, J. Phys. Chem. 76 (1972) 3020–3024, https://doi.org/10.1021/j100665a018.
[43] D.P. Santos, R.L. Longo, Molecular dynamics simulations of specific anion adsorption on sulfobetaine (SB3-14) micelles, J. Phys. Chem. B 120 (2016) 2771–2780, https://doi.org/10.1021/acs.jpcb.5b12475.
[44] L.M. Grant, W.A. Ducker, Effect of substrate hydrophobicity on surface-aggregate geometry: zwitterionic and nonionic surfactants, J. Phys. Chem. B 101 (1997) 5337–5345, https://doi.org/10.1021/jp964014w.
[45] W.A. Ducker, L.M. Grant, Effect of substrate hydrophobicity on surfactant surface-aggregate geometry, J. Phys. Chem. 100 (1996) 11507–11511, https://doi.org/10.1021/jp9607024.
[46] S.Y. Park, C.J. Barrett, M.F. Rubner, A.M. Mayes, Anomalous adsorption of polyelectrolyte layers, Macromolecules 34 (2001) 3384–3388, https://doi.org/10.1021/ma001601d.
[47] B. Schoeler, G. Kumaraswamy, F. Caruso, Investigation of the influence of polyelectrolyte charge density on the growth of multilayer thin films prepared by the layer-by-layer technique, Macromolecules 35 (2002) 889–897, https://doi.org/10.1021/ma011349p.
[48] J. Choi, M.F. Rubner, Influence of the degree of ionization on weak polyelectrolyte multilayer assembly, Macromolecules 38 (2005) 116–124, https://doi.org/10.1021/ma048596o.
[49] E.J. Shepherd, J.A. Kitchener, 474. The ionization of ethyleneimine and polyethyleneimine, J. Chem. Soc. (1956) 2448–2452.
[50] M.Y. Lin, H. Lindsay, D.A. Weitz, R.C. Ball, R. Klein, P. Meakin, Universality in colloid aggregation, Nature 339 (1989) 360.
[51] D.A. Weitz, J.S. Huang, M.Y. Lin, J. Sung, Limits of the fractal dimension for irreversible kinetic aggregation of gold colloids, Phys. Rev. Lett. 54 (1985) 1416.
[52] S. Bandini, D. Vezzani, Nanofiltration modeling: the role of dielectric exclusion in membrane characterization, Chem. Eng. Sci. 58 (2003) 3303–3326, https://doi.org/10.1016/S0009-2509(03)00212-4.
[53] R. Epsztein, E. Shaulsky, N. Dizge, D.M. Warsinger, M. Elimelech, Role of ionic charge density in donnan exclusion of monovalent anions by nanofiltration, Environ. Sci. Technol. 52 (2018) 4108–4116, https://doi.org/10.1021/acs.est.7b06400.
[54] S. Xia, L. Yao, Y. Zhao, N. Li, Y. Zheng, Preparation of graphene oxide modified polyamide thin film composite membranes with improved hydrophilicity for natural organic matter removal, Chem. Eng. J. 280 (2015) 720–727.
[55] L. Shan, H. Fan, H. Guo, S. Ji, G. Zhang, Natural organic matter fouling behaviors on superwetting nanofiltration membranes, Water Res. 93 (2016) 121–132.
[56] F. V Adams, E.N. Nxumalo, R.W.M. Krause, E.M. V Hoek, B.B. Mamba, Application of polysulfone/cyclodextrin mixed-matrix membranes in the removal of natural organic matter from water, Phys. Chem. Earth, Parts A/B/C 67 (2014) 71–78.
[57] N. Ates, L. Yilmaz, M. Kitis, U. Yetis, Removal of disinfection by-product precursors by UF and NF membranes in low-SUVA waters, J. Membr. Sci. 328 (2009) 104–112.
[58] Y. Zhao, N. Li, S. Xia, Polyamide nanofiltration membranes modified with Zn–Al layered double hydroxides for natural organic matter removal, Compos. Sci. Technol. 132 (2016) 84–92.
[59] P.D. Peeva, A.E. Palupi, M. Ulbricht, Ultrafiltration of humic acid solutions through unmodified and surface functionalized low-fouling polyethersulfone membranes–effects of feed properties, molecular weight cut-off and membrane chemistry on fouling behavior and cleanability, Separ. Purif. Technol. 81 (2011) 124–133.
[60] S. Xia, M. Ni, Preparation of poly (vinylidene fluoride) membranes with graphene oxide addition for natural organic matter removal, J. Membr. Sci. 473 (2015) 54–62.
[61] I.H. Alsohaimi, M. Kumar, M.S. Algamdi, M.A. Khan, K. Nolan, J. Lawler, Antifouling hybrid ultrafiltration membranes with high selectivity fabricated from

polysulfone and sulfonic acid functionalized TiO2 nanotubes, Chem. Eng. J. 316 (2017) 573–583.
[62] M. Kumar, Z. Gholamvand, A. Morrissey, K. Nolan, M. Ulbricht, J. Lawler, Preparation and characterization of low fouling novel hybrid ultrafiltration membranes based on the blends of GO– TiO2 nanocomposite and polysulfone for humic acid removal, J. Membr. Sci. 506 (2016) 38–49.
[63] L. Shan, Y. Liang, L. Prozorovska, G.K. Jennings, S. Ji, S. Lin, Multifold enhancement of loose nanofiltration membrane performance by intercalation of surfactant assemblies, Environ. Sci. Technol. Lett. 5 (2018) 668–674, https://doi.org/10.1021/acs.estlett.8b00430.
[64] N. Wang, S. Ji, G. Zhang, J. Li, L. Wang, Self-assembly of graphene oxide and polyelectrolyte complex nanohybrid membranes for nanofiltration and pervaporation, Chem. Eng. J. 213 (2012) 318–329.
[65] H. Tang, S. Ji, L. Gong, H. Guo, G. Zhang, Tubular ceramic-based multilayer separation membranes using spray layer-by-layer assembly, Polym. Chem. 4 (2013) 5621–5628.
[66] S. Yu, Q. Cheng, C. Huang, J. Liu, X. Peng, M. Liu, C. Gao, Cellulose acetate hollow fiber nanofiltration membrane with improved permselectivity prepared through hydrolysis followed by carboxymethylation, J. Membr. Sci. 434 (2013) 44–54.
[67] C.-C. Ye, F.-Y. Zhao, J.-K. Wu, X.-D. Weng, P.-Y. Zheng, Y.-F. Mi, Q.-F. An, C.-J. Gao, Sulfated polyelectrolyte complex nanoparticles structured nanoflitration membrane for dye desalination, Chem. Eng. J. 307 (2017) 526–536.
[68] W. Ding, H. Zhuo, M. Bao, Y. Li, J. Lu, Fabrication of organic-inorganic nanofiltration membrane using ordered stacking SiO2 thin film as rejection layer assisted with layer-by-layer method, Chem. Eng. J. 330 (2017) 337–344.
[69] S. Zhao, P. Song, Z. Wang, H. Zhu, The PEGylation of plant polyphenols/polypeptide-mediated loose nanofiltration membrane for textile wastewater treatment and antibacterial application, J. Taiwan Inst. Chem. Eng. 82 (2018) 42–55.
[70] H.P. Srivastava, G. Arthanareeswaran, N. Anantharaman, V.M. Starov, Performance of modified poly (vinylidene fluoride) membrane for textile wastewater ultrafiltration, Desalination 282 (2011) 87–94.
[71] S. Yu, Z. Chen, Q. Cheng, Z. Lü, M. Liu, C. Gao, Application of thin-film composite hollow fiber membrane to submerged nanofiltration of anionic dye aqueous solutions, Separ. Purif. Technol. 88 (2012) 121–129.
[72] M. Liu, Q. Chen, K. Lu, W. Huang, Z. Lü, C. Zhou, S. Yu, C. Gao, High efficient removal of dyes from aqueous solution through nanofiltration using diethanolamine-modified polyamide thin-film composite membrane, Separ. Purif. Technol. 173 (2017) 135–143.
[73] S. Zhao, Z. Wang, A loose nano-filtration membrane prepared by coating HPAN UF membrane with modified PEI for dye reuse and desalination, J. Membr. Sci. 524 (2017) 214–224, https://doi.org/10.1016/j.memsci.2016.11.035.
[74] H. Kang, J. Shi, L. Liu, M. Shan, Z. Xu, N. Li, J. Li, H. Lv, X. Qian, L. Zhao, Sandwich morphology and superior dye-removal performances for nanofiltration membranes self-assemblied via graphene oxide and carbon nanotubes, Appl. Surf. Sci. 428 (2018) 990–999.
[75] L. Yang, Z. Wang, J. Zhang, Zeolite imidazolate framework hybrid nanofiltration (NF) membranes with enhanced permselectivity for dye removal, J. Membr. Sci. 532 (2017) 76–86.
[76] P. Daraei, S.S. Madaeni, E. Salehi, N. Ghaemi, H.S. Ghari, M.A. Khadivi, E. Rostami, Novel thin film composite membrane fabricated by mixed matrix nanoclay/chitosan on PVDF microfiltration support: preparation, characterization and performance in dye removal, J. Membr. Sci. 436 (2013) 97–108.
[77] M. Elimelech, Xiaohua Zhu, A.E. Childress, Seungkwan Hong, Role of membrane surface morphology in colloidal fouling of cellulose acetate and composite aromatic polyamide reverse osmosis membranes, J. Membr. Sci. 127 (1997) 101–109, https://doi.org/10.1016/S0376-7388(96)00351-1.
[78] M. Elimelech, J. Gregory, X. Jia, Particle Deposition and Aggregation: Measurement, Modelling and Simulation, Butterworth-Heinemann, 2013.
[79] G.M. Litton, T.M. Olson, Colloid deposition kinetics with surface-active agents: evidence for discrete surface charge effects, J. Colloid Interface Sci. 165 (1994) 522–525.
[80] C.Y. Tang, Y.-N. Kwon, J.O. Leckie, The role of foulant–foulant electrostatic interaction on limiting flux for RO and NF membranes during humic acid fouling—theoretical basis, experimental evidence, and AFM interaction force measurement, J. Membr. Sci. 326 (2009) 526–532.
[81] M. Xie, L.D. Nghiem, W.E. Price, M. Elimelech, Impact of humic acid fouling on membrane performance and transport of pharmaceutically active compounds in forward osmosis, Water Res. 47 (2013) 4567–4575.